

Galactic and Extragalactic Magnetic Fields

Rainer Beck

Max-Planck-Institut für Radioastronomie, Auf dem Hügel 69, 53121 Bonn, Germany

Abstract. The strength of the total magnetic field in our Milky Way from radio Zeeman and synchrotron measurements is about $6 \mu\text{G}$ near the Sun and several mG in dense clouds, pulsar wind nebulae, and filaments near the Galactic Center. Diffuse polarized radio emission and Faraday rotation of the polarized emission from pulsars and background sources show many small-scale magnetic features, but the overall field structure in our Galaxy is still under debate. – Radio synchrotron observations of nearby galaxies reveal dynamically important magnetic fields of $10\text{--}30 \mu\text{G}$ total strength in the spiral arms. Fields with random orientations are concentrated in spiral arms, while ordered fields (observed in radio polarization) are strongest in interarm regions and follow the orientation of the adjacent gas spiral arms. Faraday rotation of the diffuse polarized radio emission from the disks of spiral galaxies sometimes reveals large-scale patterns which are signatures of coherent fields generated by dynamos, but in most galaxies the field structure is more complicated. – Strong magnetic fields are also observed in radio halos around edge-on galaxies, out to large distances from the plane. The synchrotron scaleheight of radio halos allows to measure the mean outflow velocity of the cosmic-ray electrons. The ordered halo fields mostly form an X-shaped pattern, but no large-scale pattern is seen in the Faraday rotation data. Diffuse polarized radio emission in the outer disks and halos is an excellent tracer of galaxy interactions and ram pressure by the intergalactic medium. – Intracluster gas can also be significantly magnetized and highly polarized due to shocks or cluster mergers.

Keywords: ISM: clouds – ISM: magnetic fields – Galaxy: spiral structure – galaxies: clusters – galaxies: halos – galaxies: interactions – galaxies: ISM – galaxies: magnetic fields – radio continuum: galaxies

PACS: 98.35.Eg, 98.35.Hj, 98.38.Gt, 98.52.Nr, 98.58.Ay, 98.62.En, 98.62.Gq, 98.62.Hr, 98.65.Cw

1. INTRODUCTION

Most of the visible matter in the Universe is ionized, so that cosmic magnetic fields are quite easy to generate and, due to the lack of magnetic monopoles, hard to destroy. Magnetic fields need illumination by cosmic rays, gas or dust to be detectable. Large regions in the Universe may be permeated by “dark” magnetic fields. In spite of our increasing knowledge on magnetic fields, many important questions, especially the origin and evolution of magnetic fields, their first occurrence in young galaxies, or the existence of large-scale intergalactic fields remained unanswered.

Results from observations and modeling revealed that magnetic fields are a major agent in the interstellar and intracluster media. They affect thermal conduction in galaxy clusters and their evolution [2]. They contribute significantly to the total pressure which balances the gas disk against gravitation. They affect the dynamics of the turbulent interstellar medium (ISM) [37] and the gas flows in spiral arms [56]. The shock strength in spiral density waves is decreased and structure formation is reduced in the presence of strong fields [39]. The interstellar fields are closely connected to gas clouds. Magnetic fields stabilize gas clouds and reduce the star-formation efficiency to the observed low values [116, 146]. On the other hand, magnetic fields are essential for the onset of star formation as they enable the removal of angular momentum from the protostellar cloud via ambipolar diffu-

sion [75]. *MHD turbulence* distributes energy from supernova explosions within the ISM [134] and drives field amplification and ordering via a *dynamo* [8]. *Magnetic reconnection* is a possible heating source for the ISM and halo gas [20, 160]. Magnetic fields also control the density and distribution of cosmic rays in the ISM. Cosmic rays accelerated in supernova remnants can provide the pressure to drive a *galactic outflow* and buoyant loops of magnetic fields via the *Parker instability* [69]. Parker loops can in turn drive a fast dynamo [67, 111]. Outflows from starburst galaxies in the early Universe may have magnetized the intergalactic medium [97]. Understanding the interaction between the gas and the magnetic field is a key to understand the physics of galaxy disks and halos and the evolution of galaxies.

2. THE TOOLS TO MEASURE MAGNETIC FIELDS

Polarized emission at optical, infrared, submillimeter and radio wavelengths holds the clue to magnetic fields in galaxies. Optical polarization is a result of extinction by elongated dust grains in the line of sight which are aligned in the interstellar magnetic field (the *Davis-Greenstein effect*). The \mathbf{E} -vector points parallel to the field. However, light can also be polarized by scattering, a process unrelated to magnetic fields and hence a contamination which is difficult to subtract. Optical polariza-

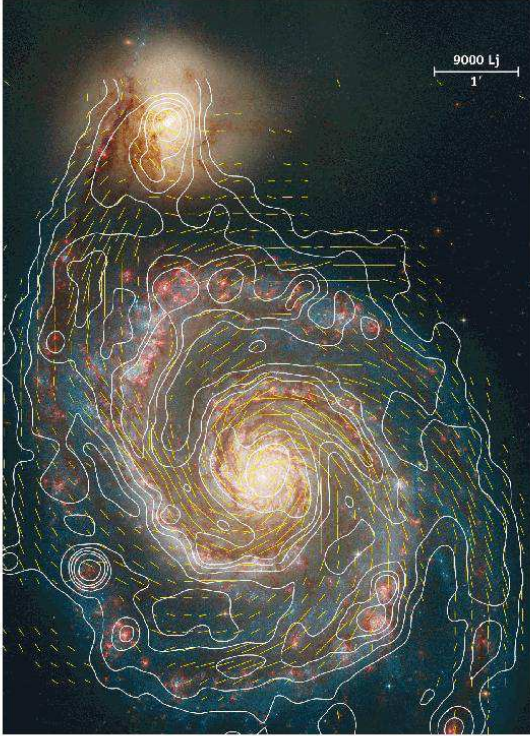


FIGURE 1. HST image of the spiral galaxy M 51, overlaid by contours of the intensity of total radio emission at 6.2 cm wavelength and B-vectors, combined from data from the VLA and Effelsberg 100m telescopes and smoothed to 15'' resolution (Fletcher & Beck, in prep.) (Graphics: Sterne und Weltraum. Copyright: MPIfR Bonn and Hubble Heritage Team).

tion surveys of stars yielded the large-scale structure of the field in the local and nearby spiral arms of our Galaxy [155]. Polarized diffuse light allowed to map magnetic field patterns also in nearby galaxies, e.g. in M 51 [126].

Polarized emission from elongated dust grains at infrared and submillimeter wavelengths is not affected by scattered light. The B-vector points parallel to the magnetic field, useful to map the structure of magnetic fields in gas clouds [35] and the halo of M 82 [59].

Most of what we know about galactic and intergalactic magnetic fields comes through the detection of radio waves. *Zeeman splitting* of radio spectral lines is the best method to directly measure the field strength [33] in gas clouds of the Milky Way (Sect. 10), OH masers in starburst galaxies [124], and in dense HI clouds in distant galaxies on the line of sight towards bright quasars [156].

The intensity of *synchrotron emission* is a measure of the number density of cosmic-ray electrons in the relevant energy range and of the strength of the total magnetic field component in the sky plane. Polarized emission emerges from ordered fields. As polarization “vectors” are ambiguous by 180°, they cannot distinguish *reg-*

ular fields with a constant direction within the telescope beam from *anisotropic fields* which are generated from turbulent magnetic fields by compressing or shearing gas flows and frequently reverse their direction on small scales. Unpolarized synchrotron emission indicates *turbulent fields* with random directions which have been tangled or generated by turbulent gas flows.

The intrinsic degree of linear polarization of synchrotron emission is about 75%. The observed degree of polarization is smaller due to the contribution of unpolarized thermal emission, which may dominate in star-forming regions, by *Faraday depolarization* along the line of sight and across the beam [131], and by geometrical depolarization due to variations of the field orientation across the beam.

At short radio wavelengths the orientation of the observed B-vector is parallel to the field orientation, so that the magnetic patterns of many galaxies could be mapped directly [4]. The orientation of the polarization vectors is changed in a magnetized thermal plasma by *Faraday rotation*. The rotation angle increases with the plasma density, the strength of the component of the field along the line of sight and the square of the observation wavelength. As the rotation angle is sensitive to the sign of the field direction, only regular fields can give rise to Faraday rotation, while anisotropic and random fields do not. For typical plasma densities and regular field strengths in the interstellar medium of galaxies, Faraday rotation becomes significant at wavelengths larger than a few centimeters. Measurements of the Faraday rotation from multi-wavelength observations allow to determine the strength and direction of the regular field component along the line of sight. Its combination with the total intensity and the polarization vectors can yield the three-dimensional picture of the magnetic field and allows to distinguish the three field components: regular, anisotropic and random.

Faraday rotation in foreground objects against the diffuse polarized background (Milky Way or a radio galaxy) may cause depolarization, generating a *Faraday shadow* or *Faraday screen* which also allow to estimate the regular field strength [49, 158].

3. DYNAMOS

The origin of the first magnetic fields in the Universe is still a mystery [154]. Protogalaxies probably were already magnetic due to field ejection from the first stars or from jets generated by the first black holes [119]. A large-scale primordial field in a young galaxy is hard to maintain because the galaxy rotates differentially, so that field lines get strongly wound up during galaxy evolution, in contrast to the observations which show significant pitch angles. This calls for a mechanism to sus-

tain and organize the magnetic field. The most promising mechanism is the dynamo [8, 22] which transfers mechanical into magnetic energy.

The *mean-field $\alpha\Omega$ -dynamo*, driven by turbulent gas motions and differential rotation, generates a large-scale regular field. Its pattern is described by modes of different azimuthal symmetry in the disk and vertical symmetry perpendicular to the disk plane. Several modes can be excited in the same object.

In spherical, rotating bodies like stars, planets or galaxy halos, the strongest mode is oscillatory and consists of a toroidal field with a sign reversal across the equatorial plane (vertically *antisymmetric* mode A0) and a poloidal dipolar field which is continuous across the plane but reverses its parity with time.

In flat, rotating objects like galaxy disks, the strongest mode consists of a toroidal field, which is symmetric with respect to the plane and has the azimuthal symmetry of an *axisymmetric* spiral in the plane without sign reversals (vertically *symmetric* mode S0) and a weaker poloidal field of quadrupolar structure with a reversal of the vertical field component across the equatorial plane [43]. The next strongest mode is of *bisymmetric* spiral shape in the plane (mode S1) with two sign reversals, followed by more complicated modes [3].

The standard mean-field $\alpha\Omega$ -dynamo in galaxy disks amplifies the field and builds up large-scale coherent fields within a few 10^9 yr [1, 8]. The driving force for the α effect can be supernova explosions [45, 60] or cosmic-ray driven Parker loops [67, 68, 105, 111].

In a spiral galaxy with disk and halo the more dynamo-active region determines the global mode, so that either a steady disk mode or an oscillatory halo mode is expected [106]. The oscillation timescales are very long for galaxies and cannot be determined by observations.

Kinematical dynamo models including the velocity field of a global galactic outflow predict field structures which are parallel to the plane in the inner disk, but open radially outwards, depending on the outflow speed and direction [21]. Some models yield oscillatory modes, but with a sufficiently fast outflow the oscillating mode may change into a steady one. However, for very fast outflows the advection time for the field becomes smaller than the dynamo amplification time, so that the dynamo action is not efficient and the field becomes frozen into the flow. Dynamical models are needed, including the interplay between the gas flow and the magnetic field.

The mean-field dynamo generates large-scale helicity with a non-zero mean in each hemisphere. As total helicity is a conserved quantity, the dynamo is quenched by the small-scale fields with opposite helicity unless these are removed from the system [129]. It seems that *outflows* are essential for an effective mean-field dynamo.

The small-scale or *fluctuation dynamo* [22] does not need general rotation, only turbulent gas motions. It am-

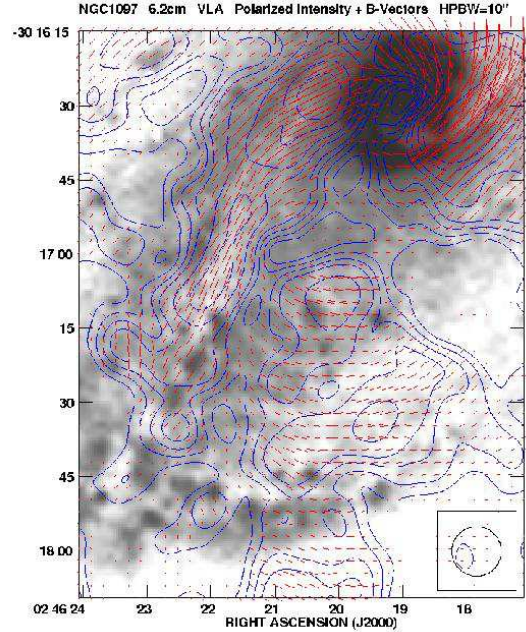


FIGURE 2. Polarized radio emission (contours) and B-vectors of the barred galaxy NGC 1097, smoothed to $10''$ resolution, observed at 6 cm wavelength with the VLA [10]. The background optical image is from Halton Arp (Copyright: MPIfR Bonn and Cerro Tololo Observatory).

plifies weak seed fields to the energy density level of turbulence within less than 10^9 yr in galaxy disks [1, 13] and within about $5 \cdot 10^9$ yr in the intracluster medium of galaxy clusters [18, 135].

4. MAGNETIC FIELDS IN SPIRAL AND BARRED GALAXIES

The strength of the total magnetic field can be determined from the intensity of the total synchrotron emission, assuming *energy equipartition* between the energy densities of the total magnetic field and the total cosmic rays, with a ratio K between the numbers of cosmic-ray protons and electrons in the relevant energy range (usually $K \simeq 100$). The equipartition assumption seems to be valid in galaxies on large scales in space and time, but deviations occur locally. In regions where electrons lost already a significant fraction of their energy, e.g. in strong magnetic fields or radiation fields, or far away from their places of origin, K is > 100 , so that the standard value of 100 yields an underestimate [12]. On the other hand, in case of fluctuations in field strength along the line of sight or across the telescope beam, the equipartition value is an overestimate [14].

The typical average equipartition strength of the total

magnetic field in spiral galaxies is about $10 \mu\text{G}$. Radio-faint galaxies like M 31 and M 33, our Milky Way’s neighbors, have weaker total magnetic fields (about $5 \mu\text{G}$), while gas-rich galaxies with high star-formation rates, like M 51 (Fig. 1), M 83 and NGC 6946, have average total field strengths of $15 \mu\text{G}$. The strongest fields ($50 - 100 \mu\text{G}$) are found in starburst galaxies, like M 82 [84] and the “Antennae” NGC 4038/9 [28], and in nuclear starburst regions, like in the centers of NGC 1097 and other barred galaxies [10]. In starburst galaxies, however, the equipartition field strength per average gas surface density is much lower than in normal spirals. This indicates strong energy losses of the cosmic-ray electrons, so that the equipartition field strength is probably underestimated by a factor of a few [140]. Recently, a field strength of $84 \mu\text{G}$ was detected in a distant galaxy at $z=0.692$ by the Zeeman effect in the HI line seen in absorption against a quasar [156].

The mean energy densities of the magnetic field and of the cosmic rays in NGC 6946 and M 33 are $\simeq 10^{-11} \text{ erg cm}^{-3}$ and $\simeq 10^{-12} \text{ erg cm}^{-3}$, respectively [5, 138], about 10 times larger than that of the ionized gas, but similar to that of the turbulent gas motions across the whole star-forming disk. The magnetic energy may even dominate in the outer disk of NGC 6946.

Spiral arms observed in total radio emission appear very similar to those observed in the far-infrared. The total equipartition field strength in the arms can be up to $30 \mu\text{G}$. The degree of radio polarization within the spiral arms is only a few %; hence the field in the spiral arms must be mostly tangled or randomly oriented within the telescope beam, which typically corresponds to a few 100 pc. Random fields in spiral arms are probably generated by turbulent gas motions due to supernovae [37], turbulence due to spiral shocks [39] or the turbulent dynamo [22]. In contrast, the ordered (regular and/or anisotropic) fields traced by the polarized synchrotron emission are generally strongest ($10 - 15 \mu\text{G}$) in the regions *between* the optical spiral arms, oriented parallel to the adjacent optical spiral arms. In several galaxies the field forms *magnetic arms* between the optical arms, like in NGC 6946 [5]. These are probably generated by the mean-field dynamo (see below). In galaxies with strong density waves some of the ordered field is concentrated at the inner edge of the spiral arms, e.g. in M 51 (Fig. 1 and [112]), but the arm–interarm contrast of the ordered field is small, much smaller than that of the random field.

The ordered magnetic field forms spiral patterns in almost every galaxy [4], even in ringed galaxies [30] and in flocculent galaxies lacking optical spiral structure [130]. Hence, the field lines generally do *not* follow the (almost circular) gas flow and need dynamo action to obtain the required radial field components. Spiral fields with large pitch angles are also observed in central regions of galaxies and in circum-nuclear gas rings [10].

On the other hand, in galaxies with massive bars the field lines seem to follow the gas flow. As the gas rotates faster than the bar pattern of a galaxy, a shock occurs in the cold gas which has a small sound speed, while the warm, diffuse gas is only slightly compressed. As the observed compression of the field in spiral arms and bars is also small, the ordered field is probably coupled to the warm diffuse gas and is strong enough to affect its flow [10]. Here, the polarization pattern is an excellent tracer of the gas flow in the sky plane and hence complements spectroscopic measurements. Detailed comparisons between polarimetric and spectroscopic data are required.

Spiral dynamo modes can be identified from the pattern of polarization angles and Faraday rotation measures (RM) from multi-wavelength radio observations of galaxy disks [43, 86] or from RM data of polarized background sources [132]. The disks of a few spiral galaxies indeed reveal large-scale RM patterns, as predicted. The Andromeda galaxy M 31 hosts a dominating axisymmetric disk field (mode S0) [47] which extends to at least 25 kpc distance from the center [61]. Other candidates for a dominating axisymmetric disk field are the nearby spiral IC 342 [91] and the irregular Large Magellanic Cloud (LMC) [53]. M 81 and PKS 1229-021 are the only candidates for bisymmetric fields [90, 98], but the data quality is limited. The magnetic arms in NGC 6946 can be described by a superposition of two azimuthal dynamo modes, where the dynamo wave is phase shifted with respect to the density wave [5]. However, in many observed galaxy disks no clear patterns of Faraday rotation were found. Either several dynamo modes are superimposed and cannot be distinguished with the limited sensitivity and resolution of present-day telescopes, or the timescale for the generation of large-scale modes is longer than the galaxy’s lifetime, so that most of the ordered fields traced by the polarization vectors are anisotropic (with frequent reversals).

Faraday rotation in the direction of QSOs allows to determine the field pattern in an intervening galaxy [98, 132]. This method can be applied to much larger distances than the analysis of RM of the polarized emission from the foreground galaxy itself. Faraday rotation of QSO emission in distant, intervening galaxies revealed significant regular fields of several μG strength [17, 95].

5. THE RADIO–FAR-INFRARED CORRELATION

The correlation between total radio and far-infrared (FIR) luminosities of star-forming galaxies is one of the tightest correlations known in astrophysics and a key to understand the role of magnetic fields in the interstellar medium. The correlation holds for starburst galaxies

[102] as well as for blue compact and low-surface brightness galaxies [29]. It extends over five orders of magnitude [15] and is valid to redshifts of at least 3 [127]. Only galaxies with very recent starbursts reveal significantly smaller radio-to-FIR ratios [125]. Slightly different slopes of the correlation are obtained if the FIR emission is separated into that from warm and cold dust [114].

Strongest total radio emission (tracing the total, mostly turbulent field) generally coincides with highest emission from dust and gas in the spiral arms: The correlation also holds for the local radio and FIR or mid-IR (MIR) intensities within galaxies [77, 112, 137, 148, 152]. In NGC 6946, the highest correlation of all spectral ranges is between the total radio intensity at $\lambda 6$ cm and the mid-infrared dust emission, while the correlation with the cold gas (as traced by the CO(1-0) transition) is less tight [50, 107, 148, 152]. A wavelet cross-correlation analysis for M 33 showed that the radio–FIR correlation holds for all scales down to 1 kpc [137]. The correlation breaks down below scales of about 50 pc [78] and in radio halos (Fig. 3). Note that the polarized intensity (tracing the ordered field) is anticorrelated or not correlated with all tracers of star formation [50].

It is not obvious why the dominating nonthermal radio and the thermal far-infrared intensities are so closely related. The intensity of synchrotron emission depends not only on the density of cosmic-ray electrons (CRE) which are accelerated in supernova remnants, but also on about the square of the strength of the total magnetic field B_t (its component in the sky plane, to be precise). The radio–FIR correlation requires that magnetic fields and star-formation processes are connected. If B_t is strong, most of the cosmic-ray energy is released via synchrotron emission within the galaxy, the CRE density decreases with B_t^2 and the integrated radio synchrotron luminosity depends on the CRE injection rate, not on B_t . If the thermal energy from star formation is also emitted within a galaxy via far-infrared emission by warm dust, this galaxy can be treated as a “calorimeter” for thermal and nonthermal emission. Prime candidates for “calorimeter” galaxies are those with a high star-formation rate (SFR). If B_t increases with SFR according to $B_t \propto \text{SFR}^{0.5}$, a linear radio–FIR correlation for the integrated luminosities is obtained [101, 102, 147]. However, the calorimeter model cannot explain the local correlation within galaxies.

In galaxies with low or medium SFR, synchrotron energy losses are probably unimportant and cosmic-ray electrons can leave the galaxy. To obtain a global or local radio–FIR correlation, coupling of magnetic fields to the gas clouds is needed. A scaling $B_t \propto \rho^{1/2}$ was proposed (author?) [76, 77, 108] where ρ is the average density of the neutral gas (atomic + molecular), given by the average number density of clouds within the telescope beam (not to be confused with the scaling for the internal den-

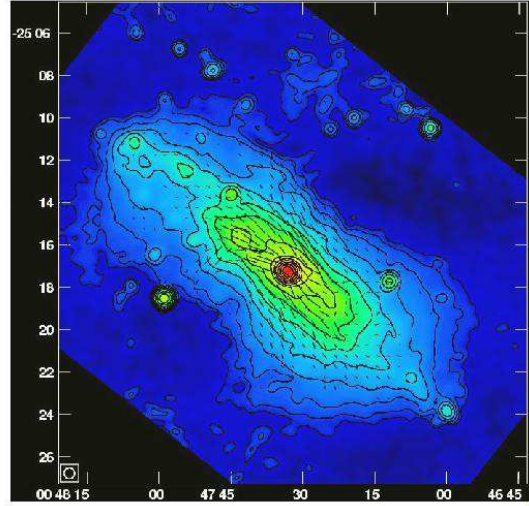


FIGURE 3. Total radio emission at 6 cm wavelength (30'' resolution) and B-vectors of the almost edge-on spiral galaxy NGC 253, combined from observations with the VLA and the Effelsberg 100m telescope [71, 72] (Copyright: AIRUB Bochum and MPIfR Bonn)

sity of molecular clouds as derived from Zeeman measurements, see Fig. 8). A nonlinear correlation (with a slope of about 1.3) between the nonthermal radio luminosity and the far-infrared luminosity from warm dust is achieved by further assuming energy equipartition between magnetic fields and cosmic rays and a Schmidt law of star formation ($SFR \propto \rho^{1.5}$) [108]. In this model the total magnetic field strength and the star-formation rate SFR are related via $B_t \propto SFR^{1/3}$.

6. RADIO HALOS OF EDGE-ON GALAXIES

Radio halos are observed around the disks of many edge-on galaxies [41, 80, 82], but their radio intensity and extent varies significantly. The halo luminosity in the radio range correlates with those in H α and X-rays [141], although the detailed halo shapes vary strongly between the different spectral ranges. These results suggest that star formation in the disk is the energy source for halo formation and the halo size is determined by the energy input from supernova explosions per surface area in the projected disk [36].

In spite of their different intensities and extents, the scale heights of radio halos at 5 GHz are $\simeq 1.8$ kpc [40, 71] with a surprisingly small scatter. Their sample of galaxies included one of the weakest halos, NGC 4565, as well as the brightest ones known, NGC 891 (Fig. 4) and NGC 253 (Fig. 3). In case of energy equipartition,

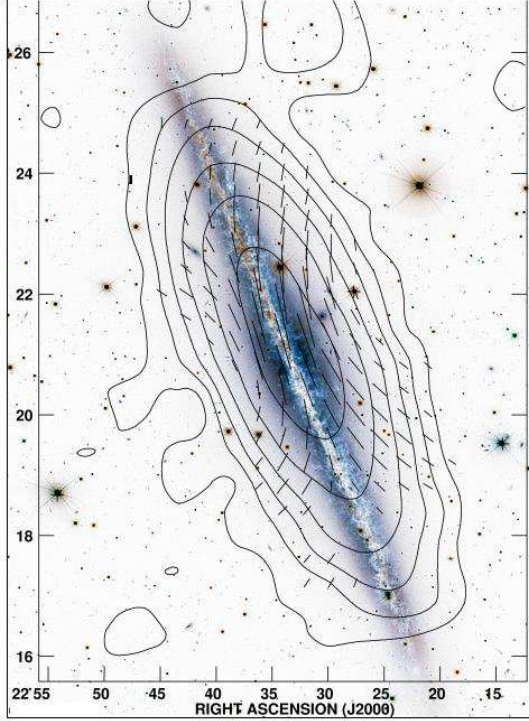


FIGURE 4. Total radio emission at 3.6 cm wavelength (84'' resolution) and B-vectors of the edge-on spiral galaxy NGC 891, observed with the Effelsberg 100m telescope [89]. The background optical image is from the CFHT (Copyright: MPIfR Bonn and CFHT/Coelum).

the scale height of the total field is at least $(3 + \alpha)$ times larger than the synchrotron scale height (where $\alpha \simeq 1$ is the synchrotron spectral index), hence ≥ 7 kpc on average. A prominent exception is NGC 4631 with the largest radio halo (field scale height of ≥ 10 kpc) observed so far [79, 81, 87] (Fig. 5). Due to the large scale heights, the magnetic energy density in halos is much higher than that of the thermal gas [42], while still lower than the dominating kinetic energy of the wind outflow.

The magnetic field scale heights are lower limits because the cosmic-ray electrons lose their energy with height above the plane, so that the equipartition formula yields too small values for the field strength [12]. The scale height of the ordered field may be even larger because the degree of linear polarization increases with height above the plane [40].

Radio halos grow in size with decreasing observation frequency which indicates that the extent is limited by energy losses of the cosmic-ray electrons, i.e. synchrotron, inverse Compton and adiabatic losses [115]. The stronger magnetic field in the central regions leads to larger synchrotron loss, leading to the “dumbbell” shape of many halos, e.g. NGC 253 [9, 72] (Fig. 3), which is

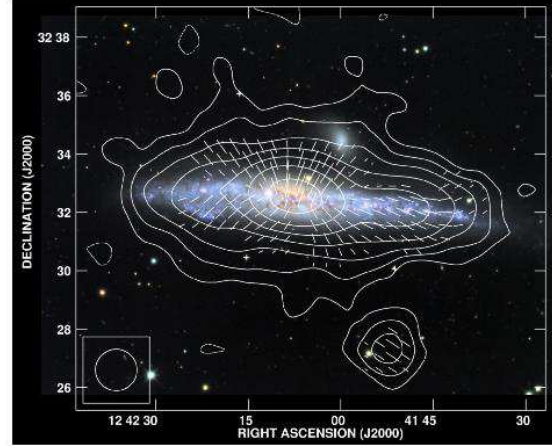


FIGURE 5. Total radio emission at 3.6 cm wavelength (84'' resolution) and B-vectors of the edge-on spiral galaxy NGC 4631, observed with the Effelsberg 100m telescope [88]. The background optical image is from the Misti Mountain Observatory (Copyright: MPIfR Bonn).

in contrast to its almost spherical X-ray halo [113]. From the radio scale heights at three frequencies and the corresponding electron lifetimes (due to synchrotron, IC and adiabatic losses) a transport speed of about 300 km/s was measured in the halo of NGC 253 [71]. The similar scale height of the radio halos around most edge-on galaxies observed so far, in spite of the different field strengths and hence different electron lifetimes, indicates that the outflow speed increases with the average field strength and the star-formation rate.

The exceptionally large radio halo around the irregular and interacting galaxies M 82 [122] and NGC 4631 [81] with their mostly radial fields in the inner region [89, 123] (Fig. 5) indicates that the wind transport is more efficient here than in other galaxies. The gravitational potential or external forces may also play a role to determine the outflow velocity.

7. MAGNETIC FIELD STRUCTURE AND FARADAY ROTATION IN RADIO HALOS

Radio polarization observations of nearby galaxies seen edge-on generally show a disk-parallel field near the disk plane [41]. High-sensitivity observations of several edge-on galaxies like NGC 891 [88] (Fig. 4), NGC 5775 [142], NGC 253 [71] (Fig. 3) and M 104 [92] show vertical field components which increase with increasing height z above and below the galactic plane and also with increasing radius [88]. These so-called X-shaped magnetic fields contain strong radial components.

The observation of X-shaped field patterns is of fundamental importance to understand the field origin in halos. The X-shape is inconsistent with the predictions from standard dynamo models without outflows (see Sect. 3). The field is probably transported from the disk into the halo by an outflow emerging from the disk. A superwind emerging from a starburst exists only in one of the edge-on galaxies observed so far, NCC 253 [70], and should produce a bipolar field pattern in the inner halo which is however not observed. A recent model for global outflows from galaxy disks (neglecting magnetic fields) shows a X-shaped velocity field [38] which may drag out the magnetic field. Improved models including magnetic fields and dynamo action are needed.

The detailed analysis of the highly inclined galaxy NGC 253 (Fig. 3) allowed a separation of the observed field into an axisymmetric disk field and a halo field inclined by about 50° [71]. Similar tilt angles are also observed at large heights in other edge-on galaxies.

In the radio halos of M 82 [122] and NGC 4631 [55] (Fig. 5) a few magnetic spurs could be resolved, connected to star-forming regions. These observations support the idea of a strong galactic outflow which is driven by regions of star formation in the inner disk.

Polarization “vectors” do not distinguish between a halo field which is sheared into elongated Parker loops or a regular field. A large-scale regular field can be measured only by Faraday rotation measures (RM). RM values in halos, e.g. in NGC 253 [9] and in NGC 4631 [87], do not show large-scale patterns, as predicted from dynamo models.

Faraday depolarization is another method to detect magnetic fields and ionized gas in galaxy halos. In NGC 891 and NGC 4631 the mean degree of polarization at 1.4 GHz increases from about 1% in the plane to about 20% in the upper halo [79]. This was modeled by depolarization due to random magnetic fields of $10 \mu\text{G}$ and $7 \mu\text{G}$ strength, ionized gas with scale heights of 0.9 kpc and 1.3 kpc, and densities in the plane of 0.03 cm^{-3} and 0.07 cm^{-3} , respectively.

8. INTERACTIONS

Interaction between galaxies or with the intergalactic medium imprints unique signatures onto magnetic fields in disks and halos. The Virgo cluster is a location of strong interaction effects. Highly asymmetric distributions of the polarized emission shows that the magnetic fields of several spirals are strongly compressed on one side of the galaxy [151, 153].

Interaction may also induce violent star-formation activity in the nuclear region or in the disk which may produce huge radio lobes due to outflowing gas and magnetic field. The lobes of the Virgo spiral NGC 4569 reach

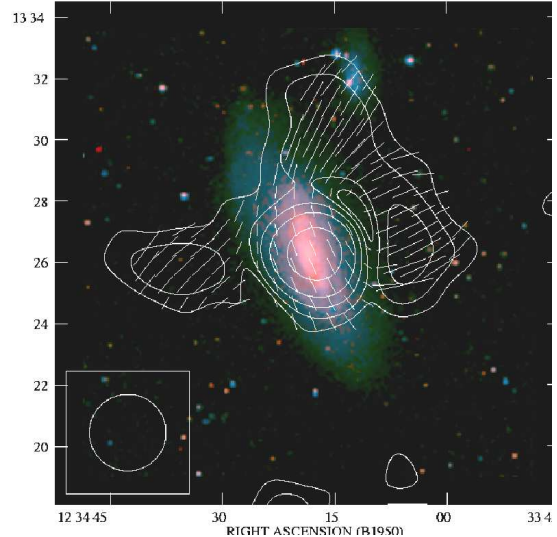


FIGURE 6. Polarized radio emission ($2.5'$ resolution) and B-vectors of the spiral galaxy NGC 4569 in the Virgo Cluster, observed at 6 cm wavelength with the Effelsberg 100m telescope [31] (Copyright: Cracow Observatory).

out to at least 25 kpc from the disk and are highly polarized [31] (Fig. 6). However, there is no indication for a recent starburst, so that the radio lobes are probably a signature of activity in the past.

Hence, polarized radio emission is an excellent tracer of interactions. As the decompression timescale of the field is very long, it keeps memory of events in the past. These are still observable if the lifetime of the illuminating cosmic-ray electrons is sufficiently large. Radio observations at low frequencies are preferable.

9. GALAXY CLUSTERS AND THE INTERGALACTIC MEDIUM

Some fraction of galaxy clusters, mostly the X-ray bright ones, has diffuse radio emission [27]. Radio *halos* are mostly unpolarized and emerge from turbulent intra-cluster magnetic fields while *relics* can be highly polarized due to merger shocks [44, 54, 57]. Magnetic fields ordered at about 1 Mpc scale were discovered in Abell 2255 [58]. Equipartition strengths of the total magnetic field range from 0.1 to $1 \mu\text{G}$ in halos and are higher in relics. On the other hand, Faraday rotation (RM) data indicate much stronger, regular fields in clusters of up to $8 \mu\text{G}$ strength [57], even $40 \mu\text{G}$ in the cores of cooling flow clusters [26] and may be dynamically important. The reason for the discrepancy in field strengths is still under discussion [12, 26, 57]. The origin of cluster fields could be outflows from AGNs, turbulent wakes or cluster mergers, possibly amplified by a turbulent dynamo

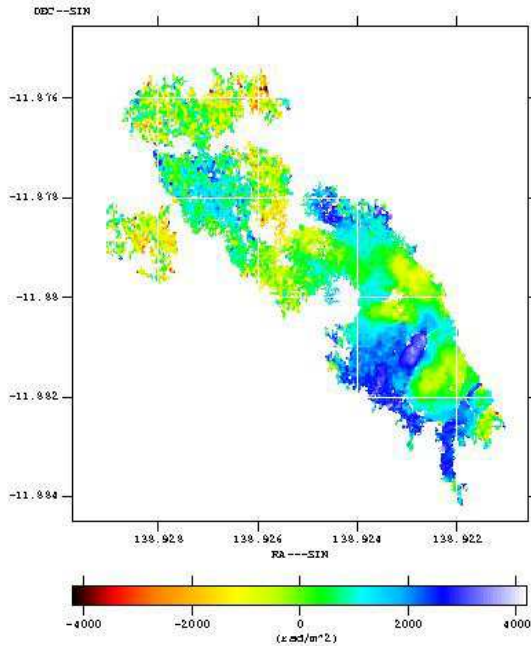


FIGURE 7. Faraday rotation map of the northern lobe of the radio galaxy Hydra A embedded in a cluster [139] (Copyright: NRAO).

[18, 135]. High-resolution RM maps of radio galaxies within clusters (Fig. 7) allow to derive the turbulence spectra of the intracluster magnetic fields which are of Kolmogorov type [149, 150].

The search for magnetic fields in the intergalactic medium (IGM) is of fundamental importance for cosmology. All “empty” space in the Universe may be magnetized. Its role as the likely seed field for galaxies and clusters and its possible relation to structure formation in the early Universe, places considerable importance on its discovery. Models of structure formation predict strong intergalactic shocks which enhance the field. Fields of $B \simeq 10^{-9}$ – 10^{-8} G are expected along filaments of 10 Mpc length with $n_e \simeq 10^{-5}$ cm $^{-3}$ electron density [94] which yield weak synchrotron emission and Faraday rotation. Their detection is a big challenge and should become possible with LOFAR and the SKA (Sect. 12).

To date there has been no detection of a general magnetic field in the IGM. Current upper limits on the average strength of the regular IGM field from Faraday rotation data suggest $|B_{\text{IGM}}| \leq 10^{-8} - 10^{-9}$ G [93]. In an intergalactic region of about 2° extent west of the Coma Cluster, containing a group of radio galaxies, enhanced synchrotron emission yields an equipartition total field strength of 0.2–0.4 μG [96]. Such fields may be typical for intergalactic filaments and should be observable with LOFAR and SKA (Sect. 12).

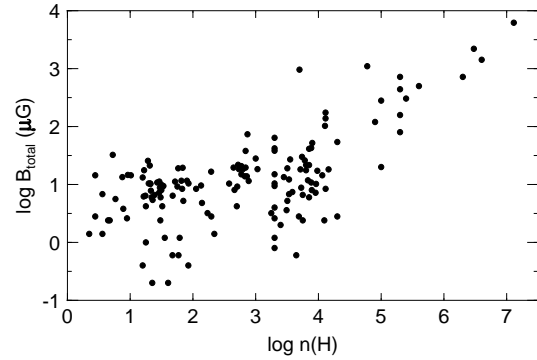


FIGURE 8. Compilation of present-day Zeeman measurements of the magnetic field in gas clouds plotted against the hydrogen volume density $n(H)$ (in cm $^{-3}$). To derive the total field B_{total} , each measured line-of-sight component was multiplied by a factor of 2 which is the average correction factor for a large sample (from [34]) (Copyright: R. M. Crutcher).

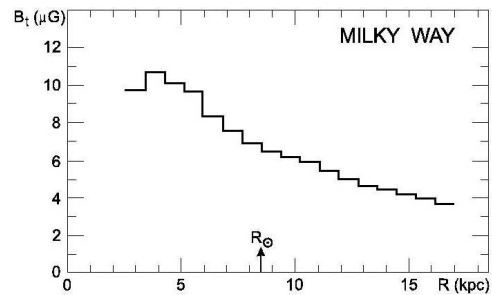


FIGURE 9. Equipartition magnetic field strength, derived from radio synchrotron emission (from Berkhuijsen, in (author?) [155]) (Copyright: MPIfR Bonn).

10. MAGNETIC FIELD STRENGTH IN THE MILKY WAY

Zeeman measurements of HI and molecular lines in gas clouds reveal the line-of-sight component of the cloud’s magnetic field. A compilation of existing data is shown in Fig. 8. The average strength for cloud densities n below about 10^3 is about $6.0 \pm 1.8 \mu\text{G}$ [74], consistent with results from synchrotron emission (see below). The energy density of the magnetic field is similar to that of the turbulent clouds motions, but larger than the thermal energy density [74], similar to the results for external galaxies (Sect. 4). For larger densities, the field strength scales with $n^{0.65 \pm 0.05}$ [34]. Zeeman splitting of OH maser lines from dense clouds yield field strengths of a few mG [46]. In dense dust clouds field strengths of about 100 μG were measured from submillimeter polarimetry [35].

Radio synchrotron data also yield an equipartition strength of the total field of 6 μG near the Sun and about 10 μG in the inner Galaxy (Fig. 9). In our Galaxy the

accuracy of the equipartition assumption can be tested, because we have independent information about the local cosmic-ray energy density from in-situ measurements and about their radial distribution from γ -ray data. Combination with the radio synchrotron data yields a local strength of the total field of $6 \mu\text{G}$ [133], the same value as derived from energy equipartition. The radial scale length of the equipartition field of $\simeq 12$ kpc is also similar to that in [133]. In the nonthermal filaments near the Galactic center the field strength may reach several $100 \mu\text{G}$ [120, 159], but the pervasive diffuse field is much weaker [110], probably $20\text{--}40 \mu\text{G}$ [100] (scaled for a proton/electron ratio of 100). Milligauss fields were also determined in the pulsar wind nebula DA 495 from a break in its synchrotron spectrum [85].

Synchrotron polarization observations in the local Galaxy imply a ratio of ordered to total field strengths of $\simeq 0.6$ [16, 73]. For a total field of $6 \mu\text{G}$ these results give $4 \mu\text{G}$ for the local ordered field component (including anisotropic random fields).

Rotation measure (RM) and dispersion measure data of pulsars give an average strength of the local coherent regular field of $1.4 \pm 0.2 \mu\text{G}$ [65, 117]. In the inner Norma arm, the average strength of the coherent regular field is $4.4 \pm 0.9 \mu\text{G}$ [63]. The regular field is claimed to be stronger in the Galactic spiral arms than in the interarm regions [64], this is however in contrast to the results from external galaxies (Sect. 4).

The values for the regular field strength derived from pulsar data are smaller than the equipartition estimates derived from polarized intensities. The latter overestimate the strength of the coherent regular field if anisotropic turbulent fields (Sect. 2) are present, but the former can also be overestimates if the small-scale fluctuations in field strength and in electron density are correlated [14] which is indicated by the analysis of RM data from extragalactic sources [136].

11. MAGNETIC FIELD STRUCTURE OF THE MILKY WAY

The all-sky distribution of extragalactic rotation measures (RM) (Fig. 10) shows the component of the large-scale field along the line of sight. The main RM peaks near the Galactic plane at longitudes of $+100^\circ$ and -110° show that the local Galactic field is oriented mainly parallel to the plane.

The maps of polarized synchrotron emission from the Milky Way from DRAO, Villa Elisa and WMAP and the new Effelsberg RM survey of polarized extragalactic sources were used to model the large-scale Galactic field [136] (Fig. 11). One large-scale reversal is required about $1\text{--}2$ kpc inside the solar radius, which agrees with the

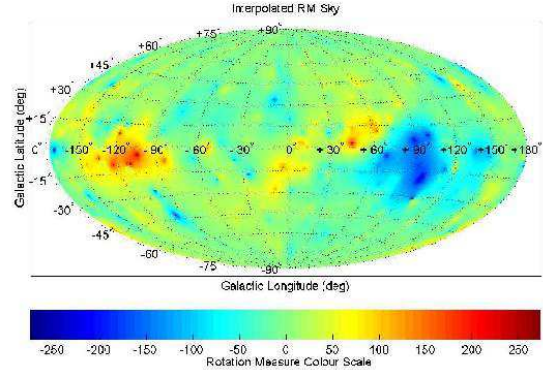


FIGURE 10. All-sky map of rotation measures in the Milky Way, generated from rotation measures towards about 800 polarized extragalactic sources, smoothed to a resolution of one square degree (from (author?) [83]) (Copyright: M. Johnston-Hollitt).

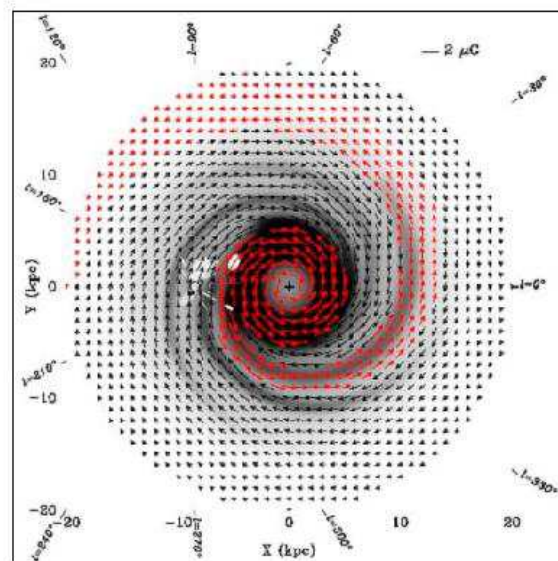


FIGURE 11. The axisymmetric model of the large-scale structure of magnetic fields in the Milky Way disk, derived from polarization surveys and rotation measures of extragalactic sources (from (author?) [136]) (Copyright: MPIfR Bonn).

detailed study of 148 RMs from extragalactic sources near the southern Galactic plane [24].

Whether the sign distribution of Zeeman measurements supports a large-scale regular field in the Galaxy is still under discussion [46, 66].

Rotation measure from pulsars allow a more detailed investigation of the field structure in the Milky Way. The field reversal inside the solar radius is also seen in the pulsar data [51, 63, 64, 117]. The local field runs clockwise (seen from the northern Galactic pole) but reverses to counter-clockwise towards the next inner spiral arm,

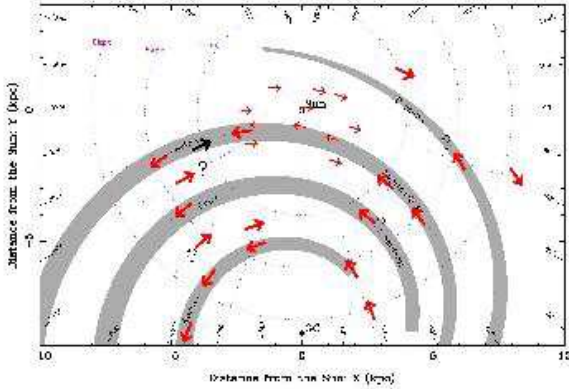


FIGURE 12. The bisymmetric model of the large-scale structure of magnetic fields in the Milky Way disk, derived from pulsar rotation measures (from (author?) [64]) (Copy-right: J. L. Han).

the Sagittarius-Carina arm, and is still counter-clockwise in the inner molecular ring.

Fig. 12 shows the location of pulsars with measured RMs within the Galactic plane and the derived directions of the large-scale field. The Sun is located between two spiral arms, the Sagittarius/Carina arm and the Perseus arm. The mean pitch angle of the arms is about -18° for the stars and -13° for all gas components [143]. Starlight polarization and pulsar RM data (Fig. 12) give a significantly smaller pitch angle of -8° for the local magnetic field [65, 73]. It is possible that the local field forms a *magnetic arm* located between two optical arms, as in NGC 6946 (Sect. 4). Differences between the pitch angles of the field and of the adjacent spiral arms of 10° – 20° were also found in the spiral galaxy M 51 [112].

A model of the Galactic field based on 554 pulsar RM values collected from several telescopes indicated reversals at several Galactic radii, possibly between each spiral arm and the adjacent interarm region [64]. The fields in the main inner arms (Carina-Sagittarius, Scutum-Crux and Norma) run counterclockwise, while the fields run clockwise in the interarm regions, in the solar neighborhood and in the outer Perseus arm. On the other hand, independent measurements of 150 pulsar RMs with the Parkes telescope (author?) [109] found safe evidence for only two reversals. The first is located about 1 kpc inside the solar radius, between the local field (clockwise field) and the Carina arm (counter-clockwise). The second reversal occurs between the Carina and Crux arms at 2–4 kpc distance from the sun towards the Galactic center. The field in the Carina arm reverses from counter-clockwise to clockwise beyond about 4 kpc distance from the sun [109], contrary to (author?) [64]. However, sub-samples of RM values above and below the Galactic plane in several regions revealed different field reversals,

which calls for caution with interpreting the data.

To account for these reversals, a circular or axisymmetric field with radial reversals [144] or a bisymmetric magnetic spiral with a small pitch angle have been proposed [65, 63, 64] (Fig. 12). However, none of the models survived a statistical test [103]. The Milky Way's field must have a complex structure which can be revealed only based on much more data.

For example, all Galactic field models so far assumed a constant pitch angle. However, experience from external galaxies shows that the field's pitch angle is not constant along the spiral arm and that the field may even slide away from the spiral arms, as observed e.g. in M 51 [112], but this cannot explain the discrepancy between the Galactic and extragalactic observations.

The existence of large-scale reversals in the Milky Way is puzzling. Very few such field reversals have been detected in external spiral galaxies. Maps of Faraday rotation of the diffuse polarized synchrotron emission are available for a couple of external spiral galaxies. Though the spatial resolution with present-day radio telescopes in external galaxies is lower, typically a few 100 pc, large-scale field reversals in the RM maps of diffuse polarized emission should be easily observable. Large-scale reversals were found only in three galaxies. In the flocculent galaxy NGC 4414 [130] and in the barred galaxy NGC 1097 [10] the line of reversal runs at about constant azimuthal angle, different from the reversals claimed for the Milky Way. A bisymmetric field structure with a large pitch angle and two azimuthal reversals on opposite sides of the disk possibly exists in M 81 [90]. The disk fields of several galaxies can be described by a mixture of dynamo modes, which may appear as a radial reversal to an observer located within the disk [128]. However, no multiple reversals along radius, like those in the Milky Way, were found so far in any external galaxy. Either the Galactic reversals are not coherent over several kpc, or they are restricted to a thin region near the Galactic plane.

Some of the Galactic reversals may not be of Galactic extent, but due to local field distortions or loops of the anisotropic turbulent field. Pulsar RMs around a star formation complex indeed revealed a field distortion which may mimic the reversal claimed to exist in the direction of the Perseus arm [104, 155].

Reversals on smaller scales are probably more frequent but also more difficult to observe in external galaxies, because higher resolution decreases the signal-to-noise ratio. Only in the barred galaxy NGC 7479, where a jet serves as a bright polarized background, several reversals on 1–2 kpc scale could be detected in the foreground disk of the galaxy [99].

The discrepancy between Galactic and extragalactic data may also be due to the different observational methods. RMs in external galaxies are averages over the line

of sight through the whole disk and halo and over the large telescope beam, and they may miss field reversals if these are restricted to a thin disk near the galaxy plane. The results in the Milky Way are based on RMs of pulsars, which trace the warm magneto-ionic medium near the plane along narrow lines of sight.

Little is known about the vertical structure of the magnetic field in the Milky Way. The vertical full equivalent thickness of the thick radio disk of the Milky Way (up to 10 kpc radius) is $\simeq 2.2$ kpc near the Sun [19] (scaled to a distance to the Galactic center of 8 kpc), corresponding to an exponential scale height of 1.6 ± 0.2 kpc which is very similar to that in spiral galaxies (Sect. 6). The local Galactic field has only a weak vertical component of $B_z \simeq 0.2 \mu\text{G}$ [65].

Dynamo models predict the generation of quadrupole or dipole fields where the toroidal component (traced by RMs) is symmetric or antisymmetric with respect to the disk plane (Sect. 3). In the Milky Way, RMs of extragalactic sources and of pulsars reveal no large-scale reversal across the plane for Galactic longitudes $l=90^\circ-270^\circ$. Thus the local field is part of a large-scale symmetric (quadrupole) field structure parallel to the Galactic plane. Towards the inner Galaxy ($l=270^\circ-90^\circ$) the RM signs are opposite above and below the plane (Fig. 10). This may indicate a global antisymmetric (dipole) mode [62]. Sun et al. (author?) [136] confirmed from their recent analysis that the halo field reverses its direction across the plane. However, the existence of a superposition of a disk field with even parity and a halo field with odd parity cannot be explained by classical dynamo theory [106].

While the large-scale field is much more difficult to measure in the Milky Way than in external galaxies, Galactic observations can trace magnetic structures to much smaller scales [121]. The 1.4 GHz all-sky polarization survey [157] reveals a wealth of structures on pc and sub-pc scales: filaments, canals, lenses and rings. Their common property is to appear only in the maps of polarized intensity, but not in total intensity. Some of these are artifacts due to strong depolarization of background emission in a foreground Faraday screen, called *Faraday ghosts* and carry valuable information about the turbulent ISM in the Faraday screen [48]. Other features are associated with real objects, like planetary nebulae [118] or the photodissociation regions of molecular clouds [158].

12. SUMMARY AND OUTLOOK

Radio synchrotron emission is a powerful tool to study the physics of galaxy disks, halos and clusters. Ordered fields in galaxy disks traced by polarized emission generally form spiral patterns, as predicted by mean-field dynamo models. In galaxies with strong non-axisymmetric



FIGURE 13. SKA reference design: aperture array for low frequencies and parabolic dishes for high frequencies (Copyright: SKA Programme Development Office and XILOSTUDIOS).

gas flows around massive bars, the ordered fields seem to follow the flow and can be used to map the velocity components of the gas flow in the sky plane which are not accessible to spectroscopic measurements.

The extent and spectral index of radio halos around galaxies and galaxy clusters give information on the transport of cosmic-ray electrons and their origin. Estimates of the electron lifetime allow an estimate of their propagation speed. Fields compressed by galaxy or cluster interactions or by ram pressure with the intergalactic gas are observable via polarized emission. The shape of the galaxy halos and their field structure allow to distinguish a global wind driven by star formation in the disk from galactic fountain or diffusion models. Faraday rotation measures trace regular fields and can test dynamo models. Faraday rotation and depolarization are also sensitive tools to detect ionized gas in galaxies, clusters and in intergalactic space.

Future radio telescopes will widen the range of observable magnetic phenomena. High-resolution, deep observations at high frequencies with the Extended Very Large Array (EVLA) and the planned Square Kilometre Array (SKA) (Fig. 13) are required to show whether the ISM and halo fields are composed of many sheared loops or are regular with dynamo-type patterns [132]. The SKA will allow to measure the Zeeman effect in much weaker magnetic fields in the Milky Way and nearby galaxies. Forthcoming low-frequency radio telescopes like the Low Frequency Array (LOFAR, Fig. 14), Murchison Widefield Array (MWA), Long Wavelength Array (LWA) and the low-frequency SKA will be suitable instruments to search for extended synchrotron radiation at the lowest possible levels in outer galaxy disks, halos and clusters, and the transition to intergalactic space. At low frequencies we will get access to the so far unex-

explored domain of weak magnetic fields in galaxy halos [7] and the population of cluster halos with very steep radio spectra [25, 27]. The detection of radio emission from the intergalactic medium will allow to probe the existence of magnetic fields in such rarified regions, measure their intensity, and investigate their origin and their relation to the structure formation in the early Universe. “Cosmic magnetism” is the title of Key Science Projects for LOFAR and SKA [6].

Multichannel spectro-polarimetric radio data allow to apply the method of RM Synthesis [23]. Faraday depolarization can be reduced and features at different distances along the line of sight can be separated. If the medium has a relatively simple structure, for example a few emitting regions and Faraday screens, *Faraday tomography* will become possible. This method will be applied to all forthcoming polarization observations.

A reliable model for the global structure of the magnetic field of the Milky Way needs a much higher number of pulsar and extragalactic RM, hence much larger sensitivity. The SKA “Magnetism” Key Science Project plans to observe an all-sky RM grid which should contain about 10^4 pulsar values with a mean spacing of $\simeq 30'$ and obtain RMs from most of these [52]. This survey will be also be used to model the structure and strength of the magnetic fields in intervening galaxies and clusters and in the intergalactic medium [11]. Deep polarization and RM observations will shed light on the origin and evolution of cosmic magnetic fields.

REFERENCES

1. T. G. Arshakian, R. Beck, M. Krause, and D. Sokoloff, *A&A*, in press, arXiv:0810.3114 (2008).
2. S. A. Balbus, and C. S. Reynolds, *ApJ* **681**, L65–L68 (2008).
3. I. Baryshnikova, A. Shukurov, A. Ruzmaikin, and D. D. Sokoloff, *A&A* **177**, 27–41 (1987).
4. R. Beck, in *Cosmic Magnetic Fields*, eds. R. Wielebinski and R. Beck, Springer, Berlin, 2005, pp. 41–68.
5. R. Beck, *A&A* **470**, 539–556 (2007).
6. R. Beck, *Adv. Radio Sci.* **5**, 399–405 (2007).
7. R. Beck, *Rev. Mex. AyA*, in press, arXiv:0804.4594 (2008).
8. R. Beck, A. Brandenburg, D. Moss, A. Shukurov, and D. Sokoloff, *Ann. Rev. A&A* **34**, 155–206 (1996).
9. R. Beck, C. L. Carilli, M. A. Holdaway, and U. Klein, *A&A* **292**, 409–424 (1994).
10. R. Beck, A. Fletcher, A. Shukurov, et al., *A&A* **444**, 739–765 (2005).
11. R. Beck, and B. M. Gaensler, in *Science with the Square Kilometer Array*, eds. C. Carilli and S. Rawlings, *New Astr. Rev.* **48**, Elsevier, Amsterdam, 2004, pp. 1289–1304.
12. R. Beck, and M. Krause, *Astron. Nachr.* **326**, 414–427 (2005).
13. R. Beck, A. D. Poezd, A. Shukurov, and D. D. Sokoloff, *A&A* **289**, 94–100 (1994).

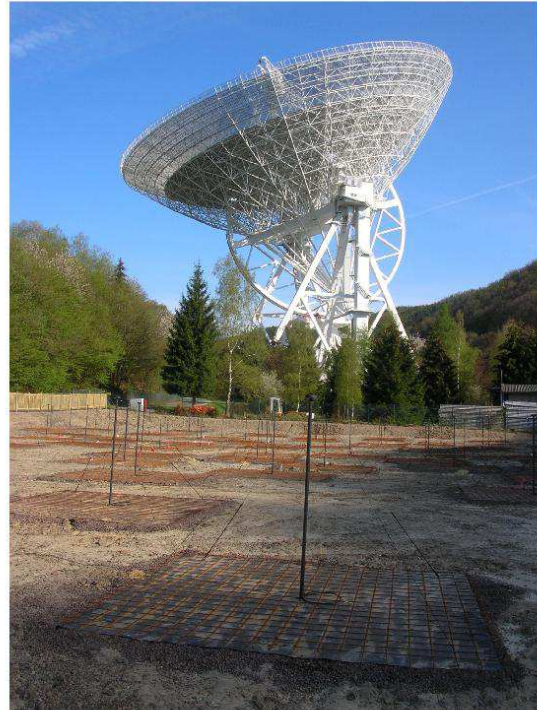


FIGURE 14. The first international LOFAR station (front) with 96 low-band antennas (30–80 MHz) next to the Effelsberg 100 m telescope (back) (Copyright: MPIfR Bonn).

14. R. Beck, A. Shukurov, D. Sokoloff, and R. Wielebinski, *A&A* **411**, 99–107 (2003).
15. E. F. Bell, *ApJ* **586**, 794–813 (2003).
16. E. M. Berkhuijsen, *A&A* **14**, 359–386 (1971).
17. M. L. Bernet, F. Miniati, S. J. Lilly, P. P. Kronberg, and M. Dessauges-Zavadsky, *Nature* **454**, 302–304 (2008).
18. S. Bertone, C. Vogt, and T. A. Enßlin, *MNRAS* **370**, 319–330 (2006).
19. K. Beuermann, G. Kanbach, and E. M. Berkhuijsen, *A&A* **153**, 17–34 (1985).
20. G. T. Birk, H. Lesch, and T. Neukirch, *MNRAS* **296**, 165–172 (1998).
21. A. Brandenburg, K. J. Donner, D. Moss, et al., *A&A* **271**, 36–50 (1993).
22. A. Brandenburg, and K. Subramanian, *Phys. Rep.* **417**, 1–209 (2005).
23. M. A. Brentjens, and A. G. de Bruyn, *A&A* **441**, 1217–1228 (2005).
24. J. C. Brown, M. Haverkorn, B. M. Gaensler, et al., *ApJ* **663**, 258–266 (2007).
25. G. Brunetti, S. Giacintucci, R. Cassano, et al., *Nature* **455**, 944–947 (2008).
26. C. L. Carilli, and G. B. Taylor, *Ann. Rev. A&A* **40**, 319–348 (2002).
27. R. Cassano, G. Brunetti, T. Venturi, et al., *A&A* **480**, 687–697 (2008).
28. K. T. Chyży, and R. Beck, *A&A* **417**, 541–555 (2004).
29. K. T. Chyży, D. J. Bomans, M. Krause, et al., *A&A* **462**, 933–941 (2007).

30. K. T. Chyży, and R. J. Buta, *ApJ* **677**, L17–L20 (2008).
31. K. T. Chyży, M. Soida, D. J. Bomans, et al., *A&A* **447**, 465–472 (2006).
32. J. M. Cordes, M. Kramer, T. J. W. Lazio, B. W. Stappers, D. C. Backer, and S. Johnston, in *Science with the Square Kilometer Array*, eds. C. Carilli and S. Rawlings, *New Astronomy Rev.* **48**, Elsevier, Amsterdam, 2004, pp. 1413–1438.
33. R. M. Crutcher, *ApJ* **520**, 706–713 (1999).
34. R. M. Crutcher, in *Magnetic Fields in the Non-masing ISM*, eds. J. M. Chapman and W. A. Baan, Cambridge Univ. Press, Cambridge, 2007, pp. 47–54.
35. R. M. Crutcher, D. J. Nutter, D. Ward-Thompson, and J. M. Kirk, *ApJ* **600**, 279–285 (2004).
36. M. Dahlem, U. Lisenfeld, and G. Golla, *ApJ* **444**, 119–128 (1995).
37. M. A. de Avillez, and D. Breitschwerdt, *A&A* **436**, 585–600 (2005).
38. C. Dalla Vecchia, and J. Schaye, *MNRAS* **387**, 1431–1444 (2008).
39. C. L. Dobbs, and D. J. Price, *MNRAS* **383**, 497–512 (2008).
40. M. Dumke, and M. Krause, in *The Local Bubble and Beyond*, eds. D. Breitschwerdt, M. J. Freyberg, and J. Trümper, Springer, Berlin, 1998, pp. 555–558 (1998).
41. M. Dumke, M. Krause, R. Wielebinski, and U. Klein, *A&A* **302**, 691–703 (1995).
42. M. Ehle, W. Pietsch, R. Beck, and U. Klein, *A&A* **329**, 39–54 (1998).
43. D. Elstner, R. Meinel, and R. Beck, *A&A Suppl.* **94**, 587–600 (1992).
44. T. A. Enßlin, P. L. Biermann, U. Klein, and S. Kohle *A&A* **332**, 395–409 (1998).
45. K. Ferrière, and D. Schmitt, *A&A* **358**, 125–143 (2000).
46. V. L. Fish, M. J. Reid, A. L. Argon, and K. M. Menten, *ApJ* **596**, 328–343 (2003).
47. A. Fletcher, E. M. Berkhuijsen, R. Beck, and A. Shukurov, *A&A* **414**, 53–67 (2004).
48. A. Fletcher, and A. Shukurov, *MNRAS* **371**, L21–L25 (2006).
49. E. B. Fomalont, K. A. Ebner, W. J. M. van Breugel, and R. D. Ekers, *ApJ* **346**, L17–L20 (1989).
50. P. Frick, R. Beck, E. M. Berkhuijsen, I. Patrikeev, *MNRAS* **327**, 1145–1157 (2001).
51. P. Frick, R. Stepanov, A. Shukurov, and D. Sokoloff, *MNRAS* **325**, 649–664 (2001).
52. B. M. Gaensler, R. Beck, and L. Feretti, in *Science with the Square Kilometer Array*, eds. C. Carilli and S. Rawlings, *New Astr. Rev.* **48**, Elsevier, Amsterdam, 2004, pp. 1003–1012.
53. B. M. Gaensler, M. Haverkorn, L. Staveley-Smith, et al., *Science* **307**, 1610–1612 (2005).
54. G. Giovannini, L. Feretti, and C. Stanghellini, *A&A* **252**, 528–537 (1991).
55. G. Golla, and E. Hummel, *A&A* **284**, 777–792 (1994).
56. G. C. Gómez, and D. P. Cox, *ApJ* **580**, 235–252 (2002).
57. F. Govoni, and L. Feretti, *Int. J. Mod. Phys. D* **13**, 1549–1594 (2004).
58. F. Govoni, M. Murgia, L. Feretti, et al., *A&A* **430**, L5–L8 (2005).
59. J. S. Greaves, W. S. Holland, T. Jenness, and T. G. Hawarden, *Nature* **404**, 732–733 (2000).
60. O. Gressel, D. Elstner, U. Ziegler, and G. Rüdiger, *A&A* **486**, L35–L38 (2008).
61. J. L. Han, R. Beck, and E. M. Berkhuijsen, *A&A* **335**, 1117–1123 (1998).
62. J. L. Han, R. N. Manchester, E. M. Berkhuijsen, and R. Beck, *A&A* **322**, 98–102 (1997).
63. J. L. Han, R. N. Manchester, A. G. Lyne, and G. J. Qiao, *ApJ* **570**, L17–L20 (2002).
64. J. L. Han, R. N. Manchester, A. G. Lyne, G. J. Qiao, and W. van Straten, *ApJ* **642**, 868–881 (2006).
65. J. L. Han, and G. J. Qiao, *A&A* **288**, 759–772 (1994).
66. J. L. Han, and J. S. Zhang, *A&A* **464**, 609–614 (2007).
67. M. Hanasz, G. Kowal, K. Otmianowska-Mazur, and H. Lesch, *ApJ* **605**, L33–L36 (2004).
68. M. Hanasz, and H. Lesch, *A&A* **332**, 77–87 (1998).
69. M. Hanasz, K. Otmianowska-Mazur, and H. Lesch, *A&A* **386**, 347–358 (2002).
70. T. M. Heckman, L. Armus, and G. K. Miley, *ApJ Suppl.* **74**, 833–868 (1990).
71. V. Heesen, R. Beck, M. Krause, and R.-J. Dettmar, *A&A*, in press, arXiv:0812.0346 (2008).
72. V. Heesen, M. Krause, R. Beck, and R.-J. Dettmar, in *The Magnetized Plasma in Galaxy Evolution*, eds. K. T. Chyży, K. Otmianowska-Mazur, M. Soida, and R.-J. Dettmar, Jagiellonian University, Kraków, 2005, pp. 156–161.
73. C. Heiles, in *Polarimetry of the Interstellar Medium*, eds. W. G. Roberge and D. C. B. Whittet, ASP Conf. Ser. **97**, Astr. Soc. Pac., San Francisco, 1996, pp. 457–474.
74. C. Heiles, and T. H. Troland, *ApJ* **624**, 773–793 (2005).
75. F. Heitsch, E. G. Zweibel, A. D. Slyz, and J. E. G. Devriendt, *ApJ* **603**, 165–179 (2004).
76. G. Helou, and M. D. Bica, *ApJ* **415**, 93–100 (1993).
77. P. Hoernes, E. M. Berkhuijsen, and C. Xu, *A&A* **334**, 57–70 (1998).
78. A. Hughes, T. Wong, R. Ekers, et al., *MNRAS* **370**, 363–379 (2006).
79. E. Hummel, R. Beck, and M. Dahlem, *A&A* **248**, 23–29 (1991).
80. E. Hummel, R. Beck, and R.-J. Dettmar, *A&A Suppl.* **87**, 309–317 (1991).
81. R. Hummel, and R.-J. Dettmar, *A&A* **236**, 33–46 (1990).
82. J. A. Irwin, J. English, and B. Sorathia, *AJ* **117**, 2102–2140 (1999).
83. M. Johnston-Hollitt, C. P. Hollitt, and R. D. Ekers, in *The Magnetized Interstellar Medium*, eds. B. Uyaniker, W. Reich, and R. Wielebinski, Copernicus, Katlenburg, 2004, pp. 13–18.
84. U. Klein, R. Wielebinski, and H. W. Morsi, *A&A* **190**, 41–46 (1988).
85. R. Kothes, T. L. Landecker, W. Reich, S. Safi-Harb, and Z. Arzoumanian, *ApJ* **687**, 516–531 (2008).
86. M. Krause, in *Galactic and Intergalactic Magnetic Fields*, eds. R. Beck, R. Wielebinski, and P. P. Kronberg, Kluwer, Dordrecht, 1990, pp. 187–196.
87. M. Krause, in *The Magnetized Interstellar Medium*, eds. B. Uyaniker, W. Reich, and R. Wielebinski, Copernicus, Katlenburg, 2004, pp. 173–182.
88. M. Krause, *Mem. Soc. Astr. Italiana* **78**, 314–316 (2007).
89. M. Krause, *Rev. Mex. AyA*, in press, arXiv:0806.2060 (2008).
90. M. Krause, R. Beck, and E. Hummel, *A&A* **217**, 17–30 (1989).

91. M. Krause, E. Hummel, and R. Beck, *A&A* **217**, 4–16 (1989).
92. M. Krause, R. Wielebinski, and M. Dumke, *A&A* **448**, 133–142 (2006).
93. P. P. Kronberg, *Rep. Prog. Phys.* **57**, 325–382 (1994).
94. P. P. Kronberg, *Astr. Nachr.* **327**, 517–522 (2006).
95. P. P. Kronberg, M. L. Bernet, F. Miniati, S. J. Lilly, M. B. Short, and D. M. Higdon, *ApJ* **676**, 70–79 (2008).
96. P. P. Kronberg, R. Kothes, C. J. Salter, and P. Perillat, *ApJ* **659**, 267–274 (2007).
97. P. P. Kronberg, H. Lesch, and U. Hopp, *ApJ* **511**, 56–64 (1999).
98. P. P. Kronberg, J. J. Perry, and E. L. H. Zukowski, *ApJ* **387**, 528–535 (1992).
99. S. Laine, and R. Beck, *ApJ* **673**, 128–142 (2008).
100. T. N. LaRosa, C. L. Brogan, S. N. Shore, T. J. Lazio, N. E. Kassim, and M. E. Nord, *ApJ* **626**, L23–L27 (2005).
101. U. Lisenfeld, H. J. Völk, and C. Xu, *A&A* **306**, 677–690 (1996).
102. U. Lisenfeld, H. J. Völk, and C. Xu, *A&A* **314**, 745–753 (1996).
103. H. Men, K. Ferrière, and J. L. Han, *A&A* **486**, 819–828 (2008).
104. D. Mitra, R. Wielebinski, M. Kramer, and A. Jessner, *A&A* **398**, 993–1005 (2003).
105. D. Moss, A. Shukurov, and D. Sokoloff, *A&A* **343**, 120–131 (1999).
106. D. Moss, and D. Sokoloff, *A&A* **487**, 197–203 (2008).
107. Ch. Nieten, N. Neininger, M. Guélin, et al., *A&A* **453**, 459–475 (2006).
108. S. Niklas, and R. Beck, *A&A* **320**, 54–64 (1997).
109. A. Noutsos, S. Johnston, M. Kramer, and A. Karastergiou, *MNRAS* **386**, 1881–1896 (2008).
110. G. Novak, in *Magnetic Fields in the Universe*, eds. E. M. de Gouveia Dal Pino et al., AIP Conf. Proc. **784**, Melville, 2005, pp. 329–339.
111. E. N. Parker, *ApJ* **401**, 137–145 (1992).
112. I. Patrikeev, A. Fletcher, R. Stepanov, et al., *A&A* **458**, 441–452 (2006).
113. W. Pietsch, A. Vogler, U. Klein, and H. Zinnecker, *A&A* **360**, 24–48 (2000).
114. D. Pierini, C. C. Popescu, R. J. Tuffs, and H. J. Völk, *A&A* **409**, 907–916 (2003).
115. M. Pohl, and R. Schlickeiser, *A&A* **234**, 147–155 (1990).
116. D. J. Price, and M. R. Bate, *MNRAS* **385**, 1820–1834 (2008).
117. R. J. Rand, and A. G. Lyne, *MNRAS* **268**, 497–505 (1994).
118. R. R. Ransom, B. Uyaniker, R. Kothes, and T. L. Landecker, *ApJ* **684**, 1009–1017 (2008).
119. M. J. Rees, in *Cosmic Magnetic Fields*, eds. R. Wielebinski and R. Beck, Springer, Berlin, 2005, pp. 1–8.
120. W. Reich, in *The Nuclei of Normal Galaxies*, eds. R. Genzel and A. I. Harris, Kluwer, Dordrecht, 1994, pp. 55–62.
121. W. Reich, in *Cosmic Polarization*, ed. R. Fabbri, Research Signpost, Kerala, 2006, pp. 91–130.
122. H.-P. Reuter, U. Klein, H. Lesch, R. Wielebinski, and P. P. Kronberg, *A&A* **256**, 10–18 (1992).
123. H.-P. Reuter, U. Klein, H. Lesch, R. Wielebinski, and P. P. Kronberg, *A&A* **282**, 724–730 (1994).
124. T. Robishaw, E. Quataert, and C. Heiles, *ApJ* **680**, 981–998 (2008).
125. H. Roussel, G. Helou, R. Beck, et al., *ApJ* **593**, 733–759 (2003).
126. S. M. Scarrott, D. Ward-Thompson, and R. F. Warren-Smith, *MNRAS* **224**, 299–305 (1987).
127. N. Seymour, T. Dwelly, D. Moss, et al., *MNRAS* **386**, 1695–1708 (2008).
128. A. Shukurov, in *Cosmic Magnetic Fields*, eds. R. Wielebinski and R. Beck, Springer, Berlin, 2005, pp. 113–135.
129. A. Shukurov, D. Sokoloff, K. Subramanian, and A. Brandenburg, *A&A* **448**, L33–L36 (2006).
130. M. Soida, R. Beck, M. Urbanik, M., and J. Braine, *A&A* **394**, 47–57 (2002).
131. D. D. Sokoloff, A. A. Bykov, A. Shukurov, E. M. Berkhuijsen, R. Beck, and A. D. Poezd, *MNRAS* **299**, 189–206 (1998) and Erratum in *MNRAS* **303**, 207–208 (1999).
132. R. Stepanov, T. G. Arshakian, R. Beck, P. Frick, and M. Krause, *A&A* **480**, 45–59 (2008).
133. A. W. Strong, I. V. Moskalenko, and O. Reimer, *ApJ* **537**, 763–784 (2000).
134. K. Subramanian, *MNRAS* **294**, 718–728 (1998).
135. K. Subramanian, A. Shukurov, and N. E. L. Haugen, *MNRAS* **366**, 1437–1454 (2006).
136. X. H. Sun, W. Reich, A. Waelkens, and T. A. Enßlin, *A&A* **477**, 573–592 (2008).
137. F. Tabatabaei, R. Beck, M. Krause, et al., *A&A* **466**, 509–519 (2007).
138. F. Tabatabaei, M. Krause, A. Fletcher, and R. Beck, *A&A* **490**, 1005–1017 (2008).
139. G. B. Taylor, and R. A. Perley, *ApJ* **416**, 554–562 (1993).
140. T. A. Thompson, E. Quataert, E. Waxman, N. Murray, and C. L. Martin, *ApJ* **645**, 186–198 (2006).
141. R. Tüllmann, D. Breitschwerdt, J. Rossa, W. Pietsch, and R.-J. Dettmar, *A&A* **457**, 779–785 (2006).
142. R. Tüllmann, R.-J. Dettmar, M. Soida, M. Urbanik, and J. Rossa, *A&A* **364**, L36–L41 (2000).
143. J. P. Vallée, *ApJ* **566**, 261–266 (2002).
144. J. P. Vallée, *ApJ* **619**, 297–305 (2005).
145. J. P. Vallée, *ApJ* **681**, 303–310 (2008).
146. E. Vázquez-Semadeni, J. Kim, and J. Ballesteros-Paredes, *ApJ* **630**, L49–L52 (2005).
147. H. J. Völk, *A&A* **218**, 67–70 (1989).
148. A. Vogler, S. C. Madden, R. Beck, et al., *A&A* **441**, 491–511 (2005).
149. C. Vogt, and T. A. Enßlin, *A&A* **412**, 373–385 (2003).
150. C. Vogt, and T. A. Enßlin, *A&A* **434**, 67–76 (2005).
151. B. Vollmer, M. Soida, R. Beck, et al., *A&A* **464**, L37–L40 (2007).
152. W. Walsh, R. Beck, G. Thuma, et al., *A&A* **388**, 7–28 (2002).
153. M. Weźgowiec, M. Urbanik, B. Vollmer, et al., *A&A* **471**, 93–102 (2007).
154. L. M. Widrow, *Rev. Mod. Phys.* **74**, 775–823 (2002).
155. R. Wielebinski, in *Cosmic Magnetic Fields*, eds. R. Wielebinski and R. Beck, Springer, Berlin, 2005, pp. 89–112.
156. A. M. Wolfe, R. A. Jorgenson, T. Robishaw, C. Heiles, and J. X. Prochaska, *Nature* **455**, 638–640 (2008).
157. M. Wolleben, T. L. Landecker, W. Reich, and R. Wielebinski, *A&A* **448**, 411–424 (2006).

158. M. Wolleben, and W. Reich, *A&A* **427**, 537–548 (2004).
159. F. Yusef-Zadeh, D. A. Roberts, W. M. Goss, D. A. Frail, and A. J. Green, *ApJ* **466**, L25–L29 (1996).
160. F. Zimmer, H. Lesch, and G. T. Birk, *A&A* **320**, 746–756 (1997).